

## Electron Relaxation in Colloidal InP Quantum Dots with Photogenerated Excitons or Chemically Injected Electrons

Jeff L. Blackburn,<sup>\*,†</sup> Randy J. Ellingson,<sup>\*,‡</sup> Olga I. Mičić,<sup>‡</sup> and Arthur J. Nozik<sup>\*,†,‡</sup>

Department of Chemistry and Biochemistry, University of Colorado, Boulder, Colorado 80309, and Center for Basic Science, National Renewable Energy Laboratory, Golden, Colorado, 80401.

Received: August 12, 2002; In Final Form: October 30, 2002

Femtosecond transient absorption spectroscopy has been used to characterize charge carrier relaxation from the second excited state (1P) to the first excited state (1S) in colloidal indium phosphide (InP) quantum dots (QDs). A three pulse experiment consisting of a visible pump, infrared pump, and white light probe was used to characterize the relaxation of photogenerated excitons, and the roles of surface chemistry and size were investigated. A two pulse experiment consisting of only the infrared pump and white light probe was used to characterize the relaxation of chemically injected electrons in the absence of holes. In the case of photogenerated excitons, two subsets of QDs were probed in the experiment, corresponding to exciton-confined and charge-separated QDs. The relaxation rates for exciton-confined and charge-separated QDs increase with decreasing QD diameter. The relaxation rates obtained for both photogenerated excitons that become charge-separated and chemically injected electrons were slowed by approximately 1 order of magnitude as compared to excitons confined to the QD core.

### Introduction

Semiconductor nanocrystals, or quantum dots (QDs), represent a remarkable class of materials with properties that bridge the gap between atomic and bulk systems. Quantum size effects arise when electronic particles are confined by potential barriers to regions of space comparable to or smaller than twice the excitonic Bohr radius. In QDs, three-dimensional confinement transforms the broad density of states characteristic of the bulk into discrete atomlike transitions and leads to a size-dependent blue shift of the semiconductor band gap. The potential and realized applications of QDs include photovoltaic cells,<sup>1–4</sup> fluorescent biological labels,<sup>5,6</sup> light-emitting diodes,<sup>7</sup> and QD lasers.<sup>8</sup>

The dynamics of charge carriers within QDs is important from both the standpoint of device performance and the general photophysics of these zero-dimensional systems.<sup>9</sup> In bulk semiconductors, the valence and conduction bands (CB) consist of a broad, densely spaced population of electronic states. Relaxation of photogenerated electrons proceeds by the emission of phonons, primarily longitudinal optical (LO) phonons, due to the large number of states available for momentum and energy conservation. In nanocrystals, excited states become discrete, adjacent electron levels can be separated by several hundred millielectronvolts, and photogenerated electrons and holes form excitons even at room temperature. In the case of InP QDs, the energy separation between the first (1S<sub>e</sub>) and the second (1P<sub>e</sub>) electron levels ranges from ~276 (50 Å QD) to ~410 meV (26 Å QD). The energy of an LO phonon in InP is 43 meV, meaning that the 1S<sub>e</sub>–1P<sub>e</sub> energy separation ranges from ~7 to 10 LO phonon energies. Relaxation by phonon emission in these systems, therefore, must occur via the emission of multiple phonons, an inefficient process suggesting a possible “phonon bottleneck”, which may slow relaxation. Evidence has been

given to support<sup>10,11</sup> and contradict<sup>12,13</sup> the phonon bottleneck; additionally, previous research has suggested a dependence on the type of phonon emitted<sup>14</sup> or the carrier involved.<sup>15</sup>

The QD surface has been shown to have a significant effect on the electronic properties of the nanocrystal. Some processes by which electrons in excited states in QDs may bypass the phonon bottleneck are defect-related processes<sup>16</sup> and Auger-like processes<sup>12,17</sup> both of which should be strongly dependent on the QD surface. Auger-like relaxation is based on the electron–hole Coulomb interaction and involves a rapid transfer of excess electronic energy to the hole, which may quickly relax through the dense spectrum of VB states.<sup>17</sup> Coulomb interactions scale inversely with the electron–hole separation, meaning that the efficiency of Auger-like relaxation should be reduced if either carrier is ejected from the QD or becomes localized on the surface of the QD.<sup>12</sup> Detailed studies of excitonic relaxation are necessary to determine the effect of surface chemistry, QD size, and carrier–carrier interactions on excitonic relaxation. Of particular interest are studies on colloidal QDs where either the electron or the hole is quenched by an acceptor molecule.<sup>10,12,18,19</sup> These studies are very useful in assigning spectral and dynamical signatures of electrons, holes, or correlated electron–hole pairs.

Steady state<sup>20–22</sup> and time-resolved<sup>10,12,23–26</sup> experiments have been performed on a variety of semiconductor QDs to explore intraband transitions involving quantized electronic states. These experiments have revealed a great deal about the nature of these transitions and their implications on mechanisms for carrier relaxation. While much attention has been given to II–VI QDs, less work has been done on III–V nanocrystals. We report on time-resolved intraband experiments on strongly confined InP QDs ranging from 26 to 50 Å in diameter. To determine the role of the surface in carrier relaxation dynamics, as-prepared nanocrystals capped in trioctylphosphine (TOP)/trioctylphosphineoxide (TOPO) are compared to TOP/TOPO-capped QDs etched with HF and to pyridine-capped QDs. To examine the

<sup>†</sup> University of Colorado.

<sup>‡</sup> National Renewable Energy Laboratory.

role of electron–hole interactions in the relaxation process, it is advantageous to track the relaxation of individual carriers. To this end, the dynamics of chemically injected electrons were examined to elucidate the role of the hole in electronic relaxation. By using infrared transient absorption (TA) spectroscopy, we are able to resolve with clarity two systems: QDs with excitons confined to the interior of the nanocrystal and QDs with holes either absent or localized at surface states. The presence of the hole in the core of the nanocrystal facilitates relaxation, and relaxation in the absence of the hole is slowed by approximately an order of magnitude.

## Experimental Section

### Synthesis and Surface Preparation of InP Nanocrystals.

Indium phosphide QDs were synthesized by standard colloidal methods as previously reported.<sup>27</sup> The reaction mixture, which consists of indium oxalate, trimethylsilylphosphine, and a 0.1:1 ratio of TOP and TOPO, was heated at 250–290 °C for 3 days, yielding an optically transparent colloidal solution. Size selective precipitation with anhydrous methanol was used to achieve a size distribution of roughly  $\pm 10\%$ , with this size distribution generally being narrower for samples with larger mean diameters. The TOP/TOPO capping group confers solubility to the QDs in organic solvents and partially passivates QD surface states. Band edge luminescence of TOP/TOPO-capped QDs remains low, however, unless the dots are etched in a dilute butanolic or ethanolic solution of HF.<sup>27</sup> Etching increases the near band edge photoluminescence by a factor of 10 or more and reduces the near-infrared emission associated with deep surface state recombination. The TOP/TOPO capping group is exchanged for pyridine by heating a dried aliquot of the QDs in  $\sim 3$  mL of pyridine at 60–70 °C for over 2 h and then letting this solution react at room temperature for  $\sim 24$  h. Addition of hexane precipitates the pyridine-capped dots, which may be centrifuged and resuspended in pyridine.

**Preparation of *n*-Type Nanocrystals.** These preparations must be performed in a purged drybox as *n*-type nanocrystals are quickly oxidized with exposure to air. As-prepared TOP/TOPO-capped InP QDs were dispersed in approximately 0.3 mL of 2,2,4,4,6,8,8-heptamethylnonane (HMN). The concentration of the solution was adjusted so that the optical density at the first excitonic peak in the linear absorption spectrum was between 0.3 and 0.6 with a path length of 500  $\mu\text{m}$ . Lower optical densities result in weaker signals for the IR-pumped intraband transition, but if the optical density is too high, insufficient transmission of probe light through the sample leads to poor signal-to-noise. To this solution was added approximately 50  $\mu\text{L}$  of 1.2 M sodium biphenyl, and the solution was vigorously stirred with a metal spatula. The solution was then quickly injected into an infrared cell for linear and TA measurements. The infrared cell consisted of two sapphire windows separated by a 0.5–0.95 mm Teflon spacer and capped with Teflon stopcocks.

**Steady State Absorption Measurements.** Steady state absorption measurements were made using a Cary 500 double beam spectrometer at a spectral resolution of 1 nm.

**TA Measurements.** TA experiments were performed on QD samples dispersed in hexane, toluene, or HMN, depending on the specific experiment. No differences, spectral or dynamical, were observed among the three solvents. The TA setup was described previously.<sup>28</sup> Briefly, a regeneratively amplified Ti: sapphire laser, operating at 989 Hz and 775 nm, is used to pump visible and infrared optical parametric amplifiers (OPAs), which are used as the experimental pump beams. The IR OPA provides

tunable near-IR pulses from 1.1 to 2.5  $\mu\text{m}$ ; the signal and idler pulses from the IR OPA are combined in a AgGaS<sub>2</sub> crystal to generate mid-IR pulses from 3 to 10  $\mu\text{m}$  by difference frequency generation. Focusing a few milliwatts of the 775 nm beam onto a 2 mm sapphire window generates the white light (WL) continuum probe.

Intraband transitions in neutral QDs coupling the first and second CB levels are accessed via a three pulse configuration, as described in ref 12. In this configuration, the visible pump pulse creates an electron–hole pair in the lowest excited state (1S) of the QD. The energy of the visible pump is chosen such that the photogenerated exciton was no more than 150 meV excess kinetic energy above the first excitonic energy for all samples:  $E_{\text{hv}} - E_{1\text{S}} \leq 0.15$  eV. The infrared photon energy is set to be resonant to the S–P energy spacing, which is determined experimentally as the energy difference between the peaks of the 1S and 1P exciton bleaches in the TA spectra. By establishing the S–P energy spacing in this manner, the infrared pulse excites the exciton from the 1S state to the 1P state, since the absorption spectra of QDs reflect transitions between energy states of confined electron–hole pairs.

The primary species measured by the TA bleaching is important to understand for the analysis of the intraband relaxation. Taking into consideration the hole's larger effective mass and closely spaced energy levels near the valence band edge, as well as the relative energy spacings of the CB and valence band (VB) levels, electrons are expected to dominate the dynamics of the TA signal. Thus, while the exciton is the primary excitation in the experiment, electrons dominate the dynamics that were measured. In QDs where the hole becomes trapped or an electron is chemically injected (discussed next), the electron is excited from its lowest level (1S<sub>e</sub>) to its next higher level (1P<sub>e</sub>). In these cases, the infrared excitation is slightly off resonance with the 1S<sub>e</sub>–1P<sub>e</sub> energy spacing. However, because of the energetic dispersion of the IR pump and energy level broadening, sufficient absorption of the IR excitation occurs within the sampling volume measured. To simplify the discussion of the three pulse experiment and because electrons should dominate the band edge bleaching, the primary excitation induced by the infrared pulse will be attributed to the electron in all cases. Thus, we will denote electron levels as S<sub>e</sub>, P<sub>e</sub>, and D<sub>e</sub> and excitonic states as S, P, and D.

After some delay with respect to the visible pump pulse,  $\Delta t_{\text{IR}}$ , the IR pump pulse promotes the 1S<sub>e</sub> electron to the 1P<sub>e</sub> level. The WL probe monitors the bleaching of the 1S transition, so that if the IR pump beam is chopped, the differential absorption resulting from only those electrons excited by the IR pump is monitored. To obtain dynamical data for electrons involved in the intraband transition, the visible and IR pump pulse are set to the desired relative delay,  $\Delta t_{\text{IR}}$ . The interband probe pulse is then delayed relative to the fixed pump pulses using an optical delay line capable of up to 300 ps delay. The delay of the interband probe pulse with respect to the visible pump will be denoted  $t_{\text{pr}}$ .

The pump fluence of the visible pump was kept low enough so that the average initial photogenerated exciton population was kept at 0.5 excitons per QD or less to avoid multiexciton interactions.<sup>28</sup> Depending on the IR pump fluence, anywhere from 15 to 50% of the electrons initially created by the visible pump pulse were reexcited by the IR pump pulse. Experiments were performed on one sample at several different IR pump fluencies, adjusted by attenuation of the IR beam, to see if this variance affected experimental results. No dependence on the

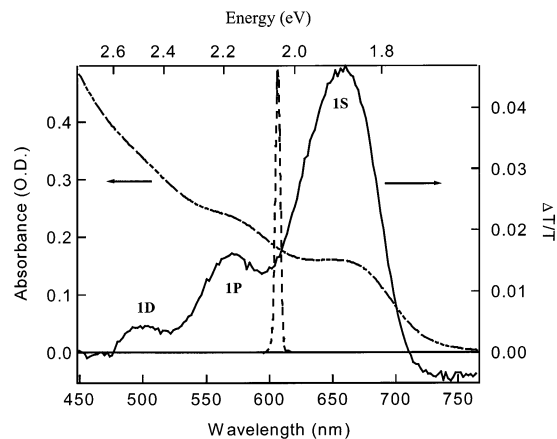


**Figure 1.** Linear absorption spectrum (dash-dotted line) and TA spectrum (solid line) for excitation at 3.2 eV,  $t_{pr} = 500$  fs. The dashed line shows the excitation pulse used in the three pulse experiment. A good size distribution for this 43 Å sample allows for the identification of three distinct transitions: 1S (1.89 eV), 1P (2.17 eV), and 1D (2.49 eV). Spectra taken on samples with broader size distributions show broader, more poorly defined features.

dynamics of relaxation with respect to IR pump fluence was observed, so all experiments were performed under conditions of the maximum IR pump fluence attainable to ensure the largest possible signal-to-noise.

The same intraband transition may be accessed in the *n*-type nanocrystals with only the IR pump pulse. In these QDs, an electron has been injected chemically into the CB by the biphenyl anion, which has a large negative redox potential; therefore, photogeneration by the visible pump pulse is unnecessary. Thus, dynamic TA experiments on *n* type nanocrystals are obtained by varying the delay of the WL probe pulse while keeping the position of the IR pump pulse fixed.

Spectral data were obtained for neutral or *n*-type nanocrystals by maintaining a fixed relative delay for the probe pulse and pump pulse(s), while spectrally dispersing the probe pulse using a CVI DK240 0.25 m monochromator.<sup>28</sup> All spectra were corrected for the chirp of the probe beam. The chirp was determined experimentally by measuring two photon absorption with the visible pump and the WL probe in a ZnO crystal. The wavelength-dependent chirp correction was entered into a table, which was used to correct spectra during acquisition.

## Results and Discussion

**Three Pulse Dynamics.** Figure 1 shows the linear absorption spectrum of 43 Å TOP/TOPO-capped InP QDs (dash-dotted line) and the TA spectrum (solid line) taken 500 fs after excitation at 3.2 eV. The dashed line shows the visible excitation pulse used in the three pulse experiment for this sample. The first excitonic transition appears as a broadened peak in the linear absorption spectrum around 1.9 eV, followed by broad shoulders corresponding to two higher energy transitions. Electronic occupation of discrete states, or state filling, leads to absorption bleaches at the positions of these transitions in the TA spectrum. Three well-resolved transitions are seen in the TA spectrum at 1.89 (1S), 2.18 (1P), and 2.49 eV (1D). The parenthetical name given to each transition is based on recent theoretical calculations, which determined the dominant character (s, p, and d, respectively) for each transition in a 42 Å InP QD.<sup>29</sup> In QD samples with mean diameters smaller than ~36 Å, only the first excitonic transition is discernible in the TA spectrum. The energy spacing between the first two transitions is calculated from the value of the corresponding bleaches and for this sample

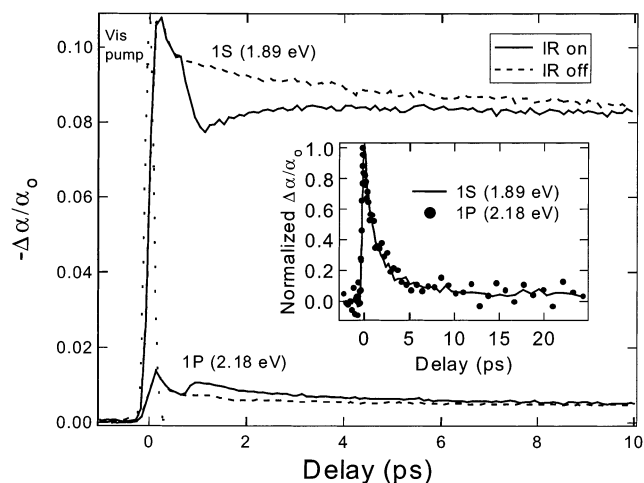


**Figure 2.** 1S and 1P bleaching dynamics measured with IR pump off (dashed lines) and IR pump on (solid lines) for 43 Å InP QDs. Note small bleaching signal at 1P transition prior to IR pump even though the visible pump does not populate this state. This bleach is due to the Stark effect created by the 1S electron. Inset: Normalized IR-modulated 1S bleach recovery and 1P bleach decay (sign reversed).

is 0.29 eV. The induced absorption occurring to the red of the 1S bleach at ~1.75 eV is attributed to the carrier-induced Stark effect, resulting from the initially created exciton shifting the 1S transition to lower energy.<sup>30</sup> At later times, a relatively flat absorption persists below 1.75 eV and stretches into the infrared; this feature is attributed to excited state absorption.

The visible pump pulse in the three pulse experiment is used to create electrons in the lowest unoccupied electron level ( $1S_e$ ) to be subsequently pumped by the IR pump pulse to the next highest electron level ( $1P_e$ ). The energy of the visible photon is such that electrons are created only in the  $1S_e$  level for the majority of QDs within the sample and not in the  $1P_e$  level, and the energy of the IR photon is adjusted to match the energy spacing between these levels calculated from the TA bleaching. For the sample shown in Figure 1, excitation at 2.04 eV ensures that electrons are created only in the  $1S_e$  level for the majority of the QDs, and IR excitation at 0.29 eV promotes the electron to the  $1P_e$  level. Probing at the energy of the 1S exciton absorption (1.89 eV for this sample) ensures that we only monitor relaxation dynamics of QDs with their 1S excitonic transition at this energy, corresponding to 43 Å diameter QDs.

The dynamics of electrons reexcited by the IR pulse may be obtained in one of two ways, as shown in Figure 2. In one method, the visible pump pulses are chopped and separate scans are taken with the IR pump on and off. Subtraction of these two scans yields the dynamics of only the electrons reexcited by the IR pulse. In the other method, the IR pulse is chopped, giving the direct dynamics of only those electrons reexcited by the IR pulse. Both methods yield the same dynamics, but IR modulation yields better signal-to-noise and is used for the entirety of these experiments.

Excitation of the  $1S_e$  electron with the infrared pump leads to a reduction in the bleaching of the 1S exciton absorption corresponding to a transition from the  $1S_e$  level and an increase in the bleaching of the 1P absorption corresponding to a transition to the  $1P_e$  level (Figure 2). The recovery (decay) of the 1S (1P) bleach corresponds to the intraband relaxation of the IR excited electrons. The inset of Figure 2 shows the normalized IR-modulated dynamics of the increase in 1P bleaching (symbols, sign reversed) and the decrease in 1S bleaching (solid line) for this 43 Å TOP/TOPO-capped InP QD sample. The dynamics of the 1S bleach recovery match the

dynamics of the 1P bleach decay and may be fit to a double exponential. The equivalent dynamics of the two processes underscores one advantage of the three pulse method for observing intraband dynamics. In normal pump–probe TA experiments, processes parallel to state filling obscure the comparison of the 1P bleach decay to the rise time of the 1S bleach. For example, the carrier-induced Stark effect contributes a fast initial rise time to the bleaching of the 1S transition, so to get realistic time constants, the relative contributions of state filling and the Stark effect must be accurately known and accounted for. This is a difficult task, and to date, the rise time of the 1S bleach has not been shown to match the decay of the 1P bleach for our InP QDs. Also, any long time constants involved in  $1P_e-1S_e$  relaxation are difficult to extract from the rise time of the 1S bleach due to convolution with the decay of the 1S bleach from recombination. As demonstrated by Figure 2, the three pulse experiment alleviates these problems, yielding dynamics that accurately reflect the intraband relaxation of electrons.

Relaxation is well fit with a double exponential, indicating the existence of two possible relaxation pathways or the existence of two subsets of excitations probed in the experiment. The coefficients for the double exponential decay for the 43 Å sample shown in Figure 2 are 540 fs (67%) and 4.0 ps (33%). With the 0.29 eV S–P energy spacing for these nanocrystals, these time constants correspond to relaxation rates of 0.54 and 0.073 eV ps<sup>-1</sup>, which are close to relaxation rates obtained for strongly confined CdSe QDs.<sup>10,12</sup> Those authors, however, also observed a very long time constant for S–P relaxation corresponding to  $\sim 10^{-3}$  eV ps<sup>-1</sup>, which we do not observe. This slow relaxation was attributed to either a phonon bottleneck in charge-separated QDs<sup>10</sup> or the accumulation of electrons in high-energy long-lived states accessed by nonlinear IR excitation.<sup>12</sup>

In ref 12, Klimov used a three pulse experiment similar to the one described here and found strongly reduced electron cooling rates when holes were captured by pyridine capping molecules after 430 fs. In this case, the relaxation time constant increased from 0.25 to 3 ps, indicating a transition from an exciton-confined QD to a charge-separated QD with the hole localized on the pyridine capping molecule. It is interesting to note the similarity of the relaxation rates obtained in refs 10 and 12 to the rates obtained on our InP QDs. This suggests the possibility that the time constants obtained in our experiments reflect two subsets of excitations probed in the experiment, corresponding to exciton-confined and charge-separated QDs. This possibility will be discussed further in the next section.

**Surface Chemistry and Charge Separation.** To investigate the role of charge separation in intraband relaxation, three different surface chemistries were explored as follows: TOP/TOPO-capped InP, HF-etched TOP/TOPO-capped InP, and pyridine-capped InP. Passivation with pyridine quenches band edge PL, ostensibly because of hole transfer to the pyridine molecule, which can readily stabilize the positive charge on the aromatic ring. In a three pulse experiment similar to ours, Klimov found that hole transfer to pyridine capping molecules on CdSe QDs occurred in 430 fs, as evidenced by the time dependence of the electron relaxation rate on the delay of the IR pump.<sup>12</sup> In Klimov's experiment, as the IR pulse was delayed from 75 to 430 fs with respect to the visible pump beam, the electronic relaxation time constant gradually increased from 250 fs to 3 ps; at a delay of 430 fs or longer, the time constant remained at 3 ps. The same experiment was performed on our InP QDs by varying  $\Delta t_{IR}$  from 75 fs to 3 ps on QDs with all three surface chemistries described above. One would expect

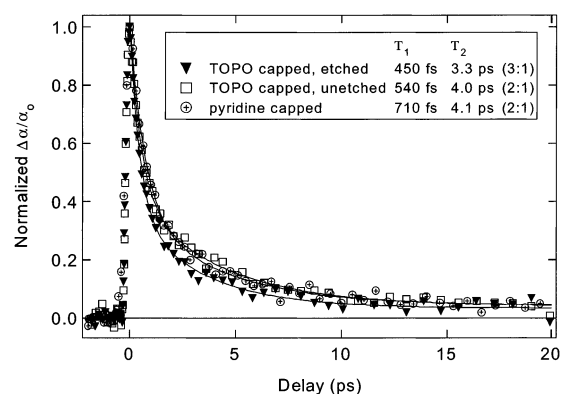


**Figure 3.** Normalized recovery of 1S bleaching in three pulse experiment for 43 Å InP QD sample with three different surface chemistries. Symbols are data, and solid lines are biexponential fits. Time constants are shown in the inset with the amplitudes for each time constant given in parentheses.

to see a relaxation rate dependent on  $\Delta t_{IR}$  for the pyridine-capped QDs if charge separation should occur and not in the case of etched or unetched TOP/TOPO-capped QDs where no charge separation is expected.

Surprisingly, it was found that the relaxation rate was completely independent of  $\Delta t_{IR}$  for all three surface chemistries examined in this study. At all IR pump delays, relaxation was biexponential with a  $\sim 500-750$  fs time constant and  $\sim 2-4$  ps time constant. With regards to a hole-trapping time scale, this implies that the hole either is never trapped or is trapped within the first 75 fs (the shortest  $\Delta t_{IR}$  studied) after photoexcitation. This lack of time dependence was expected for etched and unetched TOP/TOPO-capped QDs but is rather surprising for pyridine-capped QDs. What is also surprising is that the surface chemistry of the QD seems to play little role in the relaxation rate. Figure 3 shows the recovery of the 1S bleach for 43 Å InP QDs with the three different surface chemistries. All scans shown are taken at an IR pump delay of 1 ps, but it is important to remember that a scan taken at any  $\Delta t_{IR}$  shows the same dynamics due to the lack of time dependence. Here are three samples with very different PL quantum yields, indicative of differences in carrier trapping, but all samples show the same biexponential behavior for intraband relaxation, with slight differences in time constants for these particular scans.

The dynamics for the etched sample show a slightly higher magnitude, 75%, for the faster time component. Because the etching process increases emission by passivating surface carrier traps more completely than organic passivation, this increase suggests that the fast component of relaxation may be representative of “higher quality” QDs with more completely passivated surfaces. The results of these three pulse experiments may be compared to recent electron paramagnetic resonance (EPR) and optically detected magnetic resonance (ODMR) results<sup>31,32</sup> to gain some insight into the nature of this passivation and the effect on intraband relaxation. It was originally believed that etching with HF greatly increased band edge emission by passivating electron and hole traps at the surface with F<sup>-</sup> and H<sup>+</sup>, respectively. Following this logic, after successfully etching a sample of InP QDs with dilute HF, it would be expected that both carriers should be efficiently confined to the interior of the nanocrystal. Because of the strong electron–hole wave function overlap, relaxation should be efficient in this scenario. The EPR and ODMR studies elucidated the chemical nature of the QD surface states and their response to HF etching. It was found that two electron traps, related to indium dangling bonds, exist on the surface slightly below the CB in energy, one

radiative and one nonradiative. Etching the QD sample with HF was found to eliminate both of these traps, because of the ability of the small fluoride anion to effectively passivate these dangling bonds. A hole trap consistent with a phosphorus dangling bond was also discovered slightly above the VB. This trap state was not eliminated with HF etching, indicating poor passivation of the phosphorus dangling bonds with  $H^+$ .

The results of these experiments suggest that the severalfold increase in PL from HF etching is a result of efficient passivation of electronic surface states, but a permanent hole trap still exists on the surface of the InP QDs. Also very important is the fact that not all QDs within a given sample will possess each kind of trap. Variation of QD quality within a sample has been seen for CdSe QDs in electrostatic force microscopy (EFM) experiments performed by Krauss et al.<sup>33</sup> Those authors found that photoionization events in  $\sim 50\%$  of the CdSe QDs within their samples left a positive charge on these nanocrystals' surfaces, indicative of a surface-localized hole.

Applying these results to the dynamics shown in Figure 3, a possible model for intraband relaxation is proposed. If HF etching passivates electronic surface states but not hole surface states, then the hole can become localized at the surface in both etched and unetched TOPO-capped QDs, and the dynamics associated with these two samples will not deviate significantly. The fact that the relaxation is biexponential suggests the possibility of two subsets of QDs within the sample. Because etching has been shown to inefficiently passivate hole traps, it is proposed that two subsets of QDs are probed in this experiment: one subset in which the hole and electron are efficiently confined to the interior of the nanocrystal (hole trap absent; exciton-confined QD) and one subset in which the hole is localized at the surface of the QD on a phosphorus dangling bond (hole trap present; charge-separated QD).

With the electron and hole confined to the QD core, strong electron-hole interaction leads to efficient, fast relaxation, and in QDs where the hole is localized at the surface, increased spatial separation results in slower relaxation. The relaxation is consistent with Coulomb interaction-mediated electron-hole energy transfer proposed in previous work on CdSe<sup>12,17</sup> that occurs with reduced efficiency when the hole is trapped at the surface of the QD. The slightly larger magnitude for the fast time component for the etched sample implies that the etching process may partially passivate the hole traps. The fact that no time dependence is observed in the dynamics down to 75 fs implies that trapping at this intrinsic surface state occurs in less than 75 fs. The lack of a significant effect on coordinating ligand (i.e., TOPO and pyridine) suggests that unlike the case of CdSe QDs, holes are not trapped by pyridine in the time scale studied (75 fs to 3 ps). Electrochemical experiments on pyridine suggest that oxidation occurs around +1.6 V vs NHE.<sup>34</sup> The differing ability of pyridine to trap holes may result from the relative energetics of the VB minimum (VBM) for CdSe and InP QDs. Also possible is that hole trapping by pyridine, in contrast to trapping at P dangling bonds, occurs on a slower time scale in InP QDs than examined in this study (i.e., >3 ps). Further research is necessary to elucidate the actual quenching mechanism.

The response of the intraband dynamics to oxidation of the sample also supports the hypothesis that the slow component of relaxation results from hole trapping at P dangling bonds. EPR results show that adsorption of oxygen to the QD surface affects the hole trapping sites,<sup>32</sup> and it has been shown by X-ray photoelectron spectroscopy that oxygen directly binds to surface phosphorus atoms, passivating hole traps associated with P

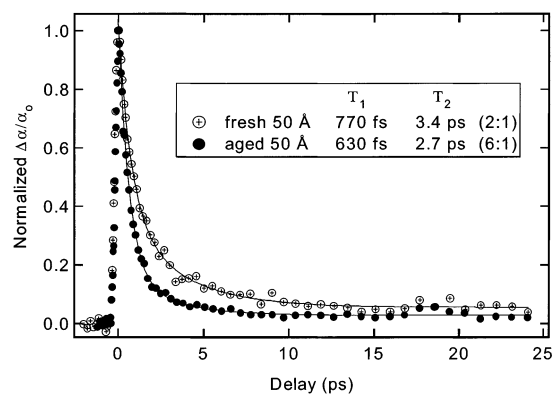


**Figure 4.** Normalized recovery of 1S bleaching in three pulse experiment for 50 Å TOP/TOPO-capped InP QDs in hexane. The fresh sample was maintained in an oxygen free glovebox and measured immediately in the sealed IR cell. The aged sample was left open to air. Time constants are shown in the inset with the amplitudes for each time constant given in parentheses.

dangling bonds.<sup>35</sup> With regards to the intraband dynamics examined in this paper, the passivation of the surface hole traps by oxidation should lead to a decrease in the magnitude of the slow time constant in the biexponential P-S dynamics. Figure 4 clearly shows a significant decrease of the magnitude of the  $\sim 4$  ps time constant upon aging in the presence of air, supporting the assignment of the slow component to QDs where the hole has become trapped at surface P dangling bonds.

**Three Pulse Spectra.** It is possible that nonlinear IR absorption, i.e., two photon absorption, can populate higher excited states or interface states that relax to the 1S state more slowly, contributing to the biexponential behavior of excitonic relaxation. The spectral positions of excited states in larger InP QDs allow our TA setup to check for these nonlinear processes. Shown in Figure 5a are TA spectra taken at different relative probe delays ( $t_{pr} - \Delta t_{IR}$ ) on a 50 Å InP QD sample at an IR pump delay ( $\Delta t_{IR}$ ) of 3 ps. The inset shows the normal pump-probe TA spectrum as a reference for the bleaching positions induced by the visible pump. Immediately following reexcitation of the 1S<sub>e</sub> electron by the IR pump, several changes in the transient bleaching spectrum are observed. An increase in absorption is observed as a broad shoulder around 750 nm (1.65 eV), the spectral position of the photoinduced absorption. Adjacent to this, at around 674 nm, is a large induced absorption corresponding to the reduction of the 1S bleaching. This is caused by the IR-induced resonant transition from the 1S<sub>e</sub> to the 1P<sub>e</sub> level and interestingly is blue-shifted by  $\sim 43$  meV from the normal 1S bleach position. After 1.05 ps, the 1S feature has shifted back to its normal position. The reason for the blue shift is unknown, but it interestingly matches the LO phonon energy in InP.

Successful promotion of the electron to the 1P<sub>e</sub> level creates an IR-induced bleach at 600 nm (2.07 eV) but also induces a bleach at 540 nm (2.30 eV), the position of the 1D. As relaxation progresses, higher energy electrons primarily populate the 1P<sub>e</sub> level and continually repopulate the 1S<sub>e</sub> level. Theoretical calculations on a 42 Å InP QD indicate that the 1D peak is made up of three separate excitonic transitions, one of which shares the 1P<sub>e</sub> electron level with the 1P exciton transition.<sup>29</sup> This implies that if the electron is promoted to the 1P<sub>e</sub> level, state filling should also produce a partial bleach in the TA spectrum for the 1D peak. This situation is a possibility for the 50 Å InP QD shown in Figure 5.

While this explanation may provide some insight into the origin of the 1D bleach, two photon absorption must also be

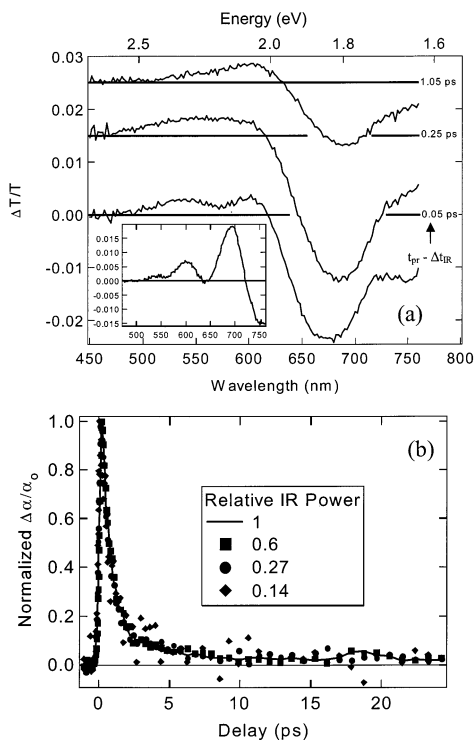


**Figure 5.** (a) TA spectra showing changes in transmission induced by the IR pump in the three pulse experiment for a 50 Å InP QD sample. Times shown are the probe delay relative to the IR pump. The IR pump is held at a 3.0 ps delay with respect to the visible pump ( $\Delta t_{\text{IR}} = 3.0$  ps), so that  $[t_{\text{pr}} - \Delta t_{\text{IR}}] = 0.05$  ps corresponds to an absolute WL probe delay of 3.05 ps with respect to the visible pump. Shown in the inset is the normal two pulse TA spectrum taken between 0.1 and 0.5 ps after excitation at 3.2 eV as a reference for the original visible-induced bleaching signals. (b) Intraband dynamics of 50 Å InP QD sample taken at  $\Delta t_{\text{IR}} = 3.0$  ps at different IR pump intensities. Relative IR power is shown in the inset. It should be noted that this sample was slightly oxidized, leading to slightly faster than normal dynamics as discussed in Figure 4.

considered. The P–D energy spacing for the larger InP QD samples is quite close to the S–P energy spacing, and for the sample in Figure 5, the two only differ by about 40 meV. It is therefore possible that a two photon absorption process could populate this 1D level, giving rise to the IR-induced absorption at 2.30 eV. The population of higher energy excited states could explain the biexponential behavior of relaxation. Studies on bulk semiconductors have shown that higher energy excitation within the central  $\Gamma$  valley allows access to lower mobility satellite valleys (X and L).<sup>36</sup> In ref 36, carrier mobility in the highly mobile  $\Gamma$  valley of bulk GaAs was measured, and it was found that due to finite scattering rates from satellite valleys back into the  $\Gamma$  valley, higher energy excitation yielded slower signal rise times. This is a feasible scenario for excitations in QDs as well. Recent theoretical calculations have found several L-derived conduction levels at energies between the  $1D_e$  and  $1P_e$  levels.<sup>29</sup> The contribution of two photon absorption to the dynamics of relaxation may be ruled out, however, by examining the dependence of the dynamics on the power of the IR beam (Figure 5b). It can be seen in this figure that when the IR power is varied over approximately an order of magnitude, the relative contributions of the fast and slow components of relaxation do not change.

#### N-Type Nanocrystals: Relaxation in the Absence of Holes.

To accurately assess the mechanisms involved in the intraband relaxation, it is helpful to view a system in which only one carrier is present. N-type nanocrystals represent a system in

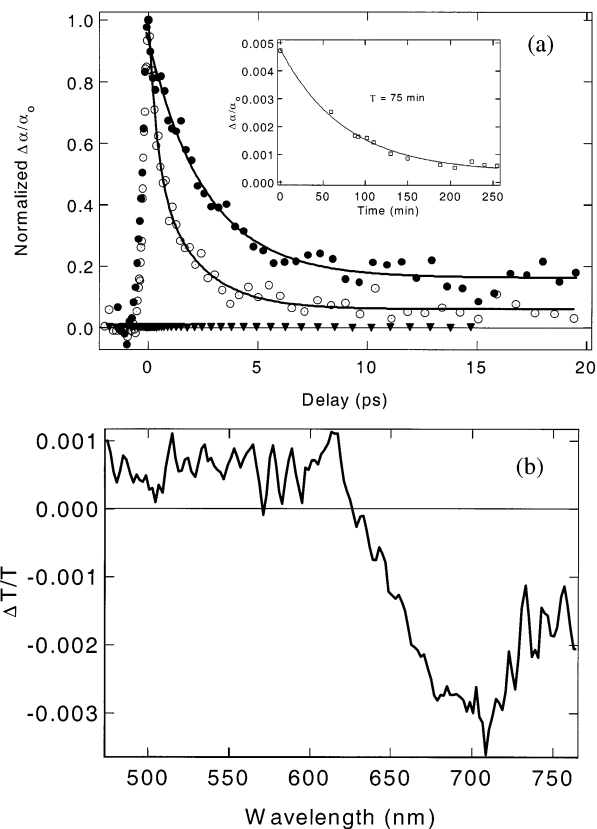


**Figure 6.** (a) TA traces comparing dynamics of 1S bleach recovery in 50 Å InP QDs. Open circles show neutral QDs where the 1S exciton is created via three pulse experiment. Closed circles show n-type QDs where 1S electron is injected chemically and pumped only with IR pulse. Triangles show neutral QDs pumped only with IR pulse. The inset shows the time evolution of the intraband transition signal in n-type QDs due to chemically injected electrons. (b) Spectral changes induced by IR pump on 50 Å InP QD treated with sodium biphenyl to inject electrons into the QD CB.

which electronic relaxation may be measured in the absence of holes. Sodium biphenyl is a very strong reducing agent, which has been shown to successfully inject electrons into the CB of CdSe QDs,<sup>20,21</sup> effectively bleaching the 1S transition and allowing an IR-induced transition to the  $1P_e$  level. Steady state absorption and luminescence experiments have elucidated important features about these systems, but to date, time-resolved techniques have not been used to follow the dynamics of the IR-induced intraband transition associated with the injected electron.

Sodium biphenyl was successfully used to inject electrons into the CB of our InP QDs. After a sample of InP QDs is treated with sodium biphenyl, the first excitonic transition is bleached indicating an electron is present in the lowest unoccupied electron level. This  $1S_e$  electron may be excited to the  $1P_e$  level with the IR pump. Figure 6a compares the dynamics of the time-resolved, IR-induced transitions in n type and neutral 50 Å TOP/TOPO-capped InP QDs. In neutral QDs (open circles), where the IR pulse induces the  $1S_e - 1P_e$  transition on a photogenerated electron, relaxation occurs biexponentially (solid fit line) as expected. Triangles represent the same sample pumped only with the IR pump. No absorption of the IR pump occurs because no electrons are present in the CB. In sharp contrast, only the IR pump is necessary to pump the  $1S_e - 1P_e$  transition in the same sample treated with sodium biphenyl (filled circles). The relaxation of electrons pumped in this experiment is fit to a single exponential (solid line) with an average time constant of 3.0 ps, corresponding to a relaxation rate of  $0.092 \text{ eV ps}^{-1}$ .

Figure 6b shows the spectral changes induced by the IR pump 300 fs after excitation. The reduction in bleaching maps out the 1S transition just as in Figure 5a for the 50 Å neutral QDs treated with the three pulse configuration. This confirms that electrons are successfully injected into the QD CB and that the two experiments monitor the same S–P transition.

Shown in the inset of Figure 6a is the disappearance of the IR-induced transition with time. The *n*-type QDs oxidize relatively quickly due to the infiltration of air into the cells, which are not entirely airtight. In the case of our InP QDs, oxidation occurs exponentially with a time constant of 75 min. This presents an experimental challenge in that TA spectra and dynamical scans must be performed immediately following treatment with sodium biphenyl. It has been shown that this oxidation rate is quenched at lower temperatures,<sup>20</sup> although we did not perform any experiments at lower temperatures for this paper.

In *n*-type QDs, no hole is present to facilitate relaxation via Auger-like electron–hole energy transfer. It is therefore expected, and observed, that the fast time constant is absent from the relaxation dynamics. This confirms that in the absence of a core-confined hole, electronic relaxation is slowed by about an order of magnitude. The relaxation rate obtained matches very closely with the relaxation rate assigned to electronic relaxation with a surface-localized hole, suggesting a similar relaxation mechanism.

A consideration of the physical environment of the QD within the sodium biphenyl-treated solution may yield some insight into this similarity. The sodium biphenyl is initially dissolved in di(ethyleneglycol) diethyl ether, which has a high dielectric constant. This solution is vigorously stirred into a solution of HMN, which has a much lower dielectric constant of  $\sim 2.0$ . Because the biphenyl anion is in large excess as compared to the QDs and the redox potential is far negative of the QD CB, electrons should be injected into the QD CB as well as electronic traps associated with the surface states mentioned earlier. This should leave an overall negative charge on the QD surface. Because of the very low dielectric constant of HMN, sodium ions are likely to associate with the negatively charged QD surface. Hence, even though no photogenerated holes are present in the *n*-type QD, electronic relaxation may be affected by the positive charge localized at the QD surface, creating a situation analogous to relaxation in neutral QDs with a surface-localized hole. Thus, similar Coulombic coupling associated with a surface-localized positive charge may be present in both cases, leading to similar relaxation rates.

Another interesting feature of the dynamics for the *n*-type InP QDs is that the 1S bleach does not fully recover following IR excitation on the time scale studied here. This could be indicative of a very slow time constant for the  $1P_e-1S_e$  relaxation that we cannot resolve due to the time constraints of the experiment mentioned above. This could result from a variation in the distribution of surface electron traps within the QD sample similar to the hole trap distribution discussed above. In this case, QDs without surface electron traps would not be left with an overall negative surface charge and would not have sodium ions associated with the surface. Thus, electronic relaxation would occur in the complete absence of Coulombic coupling, leading to slow relaxation via a phonon bottleneck. The incomplete 1S bleach recovery could also be indicative of an increased probability of photoionization due to nonlinear IR excitation in the *n*-type QDs. It is feasible that the lack of a hole in the QD could make ejection of the electron into the solvent easier than for the case where the hole is present. Neither

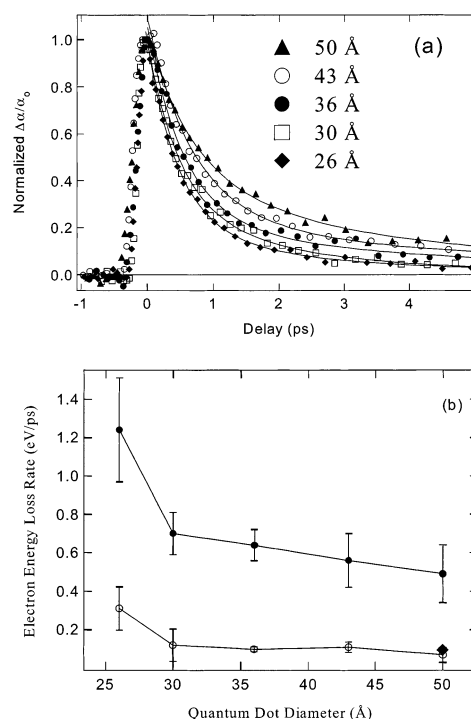


**Figure 7.** (a) Normalized recovery of 1S bleaching in three pulse experiment for five InP QD samples with different mean diameters. Symbols are data, and solid lines are biexponential fits. (b) Exciton energy loss rate as a function of QD diameter. Calculated using average values for biexponential fit and energy spacing between 1S and 1P transition. The slow component is shown as open circles, and the fast component is shown as closed circles. Also shown as the filled diamond is the energy loss rate for CB electron in *n* type QDs.

of the above hypotheses may be confirmed from these experiments and further experiments, likely at lower temperatures, are necessary to investigate this interesting feature.

**Size Dependence of Intraband Relaxation.** The model for the phonon bottleneck predicts that in smaller QDs where the  $1S_e-1P_e$  spacing becomes much larger, phonon effects may play a greater role in electronic relaxation, leading to slowed relaxation. To examine this possibility, a series of five InP QD samples ranging from 26 to 50 Å in diameter was examined with the three pulse experiment. For each sample, the photon energy of the IR pump was adjusted to be resonant with the S–P transition. For the smallest two sizes, the size distribution was too broad to observe a well-defined peak for the 1P transition. For these samples, the S–P energy spacing measured on samples of narrower size distribution in ref 37 was used. Figure 7a shows the three pulse dynamics for the five different-sized samples taken at an IR pump delay of 1 ps. As previously observed, no samples showed any time dependence of the relaxation on the IR pump delay, and all of the decays fit well to a double exponential (solid lines). Figure 7a unambiguously demonstrates a decrease in the relaxation time constants (i.e., increase in relaxation rates) with decreasing size.

Figure 7b summarizes the dependence of the fast and slow relaxation rates on QD size. Also shown as the diamond is the relaxation rate obtained for electrons in the 50 Å *n*-type QDs discussed in the previous section. Both rates increase with decreasing dot size, although the slower rate increases less rapidly. That both rates increase with decreasing QD size supports the hypothesis that the relaxation in both exciton-confined and charge-separated QDs is mediated by Coulomb electron–hole interactions. The issue of why relaxation in the

in *n*-type QDs does not proceed more slowly than  $\sim 3$  ps is a very important one that must be further explored.

## Conclusion

We have demonstrated the successful injection of electrons into the CB of InP QDs and the temporal tracking of these injected electrons by TA spectroscopy. The comparison of the dynamics of chemically injected electrons to the dynamics of photogenerated electrons shows a reduction in the electron relaxation rate by approximately 1 order of magnitude when the hole is absent or trapped at the surface of the QD. It is proposed that an intrinsic surface state related to phosphorus dangling bonds acts to trap photogenerated holes. Our results suggest that the different surface preparations for the InP QDs primarily affect midgap electron trapping sites, producing only slight variations in electronic relaxation within the CB. The size-dependent dynamics of the 1P–1S relaxation indicate relaxation rates that increase with decreasing dot size.

**Acknowledgment.** We thank the U.S. Department of Energy, Office of Science, Office of Basic Energy Sciences, Division of Chemical Sciences, Geosciences, and Biosciences for financial support and Garry Rumbles for helpful discussions.

## References and Notes

- Zaban, A.; Mičić, O. I.; Gregg, B. A.; Nozik, A. J. *Langmuir* **1998**, *14*, 3153.
- Greenham, N. C.; Poeng, X.; Alivisatos, A. P. *Phys. Rev. B* **1996**, *54*, 17628.
- Greenham, N. C.; Peng, X.; Alivisatos, A. P. *Phys. Rev. B* **1999**, *59*, 10622.
- Vogel, R.; Weller, H. *J. Phys. Chem.* **1994**, *98*, 3183.
- Bruchez, M., Jr.; Moronne, M.; Gin, P.; Weiss, S.; Alivisatos, A. *P. Science* **1998**, *281*, 2013.
- Michalet, X.; Pinaud, F.; Lacoste, T. D.; Dahan, M.; Bruchez, M. P.; Alivisatos, A. P.; Weiss, S. *Single Molecules* **2001**, *2*, 261.
- Dabbousi, B. O.; Bawendi, M. G.; Onitsuka, O.; Rubner, M. F. *Appl. Phys. Lett.* **1995**, *66*, 1316.
- Eisler, H.-J.; Sundar, V. C.; Bawendi, M. G.; Walsh, M.; Smith, H. I.; Klimov, V. *Appl. Phys. Lett.* **2002**, *80*, 4614.
- Nozik, A. J. *Annu. Rev. Phys. Chem.* **2001**, *52*, 193.
- Guyot-Sionnest, P.; Shim, M.; Matranga, C.; Hines, M. *Phys. Rev. B* **1999**, *60*, R2181.
- Murdin, B. N.; Hollingsworth, A. R.; Kamal-Saadi, M.; Kotitschke, R. T.; Ciesla, C. M.; Pidgeon, C. R.; Findlay, P. C.; Pellemans, H. P. M.; Langerak, C. J. G. M.; Rowe, A. C.; Stradling, R. A.; Gornik, E. *Phys. Rev. B* **1999**, *59*, R7817.
- Klimov, V. I.; Mikhailovsky, A. A.; McBranch, D. W.; Leatherdale, C. A.; Bawendi, M. G. *Phys. Rev. B* **2000**, *61*, R13349.
- Woggon, U.; Giessen, H.; Gindele, F.; Wind, O.; Fluegel, B.; Peyghambarian, N. *Phys. Rev. B* **1996**, *54*, 17681.
- Vollmer, M.; Mayer, E. J.; Ruhle, W. W.; Kurtenbach, A.; Eberl, K. *Phys. Rev. B* **1996**, *54*, R17292.
- Xu, S.; Mikhailovsky, A. A.; Hollingsworth, J. A.; Klimov, V. I. *Phys. Rev. B* **2002**, *65*, 045319.
- Schroeter, D. F.; Griffiths, D. J.; Sercel, P. C. *Phys. Rev. B* **1996**, *54*, 1486.
- Efros, A. L.; Kharchenko, V. A.; Rosen, M. *Solid State Commun.* **1995**, *93*, 281.
- Burda, C.; Link, S.; Mohamed, M.; El-Sayed, M. *J. Phys. Chem. B* **2001**, *105*, 12286.
- Burda, C.; Green, T. C.; Link, S.; El-Sayed, M. *J. Phys. Chem. B* **1999**, *103*, 1783.
- Shim, M.; Wang, C.; Guyot-Sionnest, P. *J. Phys. Chem. B* **2001**, *105*, 2369.
- Shim, M.; Guyot-Sionnest, P. *Nature* **2000**, *407*, 981.
- Wang, C.; Shim, M.; Guyot-Sionnest, P. *J. Science* **2001**, *291*, 2390.
- Klimov, V. I.; McBranch, D. W. *Phys. Rev. Lett.* **1998**, *80*, 4028.
- Shim, M.; Shilov, S. V.; Braiman, M. S.; Guyot-Sionnest, P. *J. Phys. Chem. B* **2000**, *104*, 1494.
- Shim, M.; Guyot-Sionnest, P. *J. Phys. Rev. B* **2001**, *64*, 245342.
- Guyot-Sionnest, P. J.; Hines, M. A. *Appl. Phys. Lett.* **1998**, *72*, 686.
- Nozik, A. J.; Mičić, O. I. Colloidal Quantum Dots of II–V Semiconductors. In *Handbook of Nanostructured Materials and Nanotechnology*; Nalwa, H. S., Ed.; Academic Press: New York, 2000; Vol. 3, p 427.
- Ellingson, R. J.; Blackburn, J. L.; Yu, P.; Rumbles, G.; Mičić, O. I.; Nozik, A. J. *J. Phys. Chem. B* **2002**, *106*, 7758.
- Ellingson, R. J.; Blackburn, J. L.; Mičić, O. I.; Fu, X.; Nozik, A. J. Unpublished results.
- Klimov, V. I. *J. Phys. Chem. B* **2000**, *104*, 6112.
- Langof, L.; Ehrenfreund, E.; Lifshitz, E.; Mičić, O. I.; Nozik, A. J. *J. Phys. Chem. B* **2002**, *106*, 1606.
- Mičić, O. I.; Nozik, A. J.; Lifshitz, E.; Rajh, T.; Poluektov, O. G.; Thurnauer, M. C. *J. Phys. Chem. B* **2002**, *106*, 4390.
- Krauss, T. D.; O'Brien, S.; Brus, L. E. *J. Phys. Chem. B* **2001**, *105*, 1725.
- Turner, W. R.; Elving, P. J. *Anal. Chem.* **1965**, *37*, 467.
- Guzelian, A. A.; Katari, J. E. B.; Kadavanich, A. V.; Banin, U.; Hamad, K.; Juban, E.; Alivisatos, A. P.; Wolters, R. H.; Arnold, C. C.; Heath, J. R. *J. Phys. Chem.* **1996**, *100*, 7212.
- Beard, M. C.; Turner, G. M.; Schmuttenmaer, C. A. *Phys. Rev. B* **2000**, *62*, 15764.
- Mičić, O. I.; Cheong, H. M.; Fu, H.; Zunger, A.; Sprague, J. R.; Mascarenhas, A.; Nozik, A. J. *J. Phys. Chem. B* **1997**, *101*, 4904.